Since January 2020 Elsevier has created a COVID-19 resource centre with free information in English and Mandarin on the novel coronavirus COVID-19. The COVID-19 resource centre is hosted on Elsevier Connect, the company's public news and information website.

Informatics in Medicine Unlocked 33 (2022) 101081

Contents lists available at ScienceDirect

Informatics in Medicine Unlocked

journal homepage: www.elsevier.com/locate/imu

Swarming morlet wavelet neural network procedures for the mathematical robot system

Peerapongpat Singkibud [a], Zulqurnain Sabir [b,c], Irwan Fathurrochman [d], Sharifah E. Alhazmi [e], Mohamed R. Ali [f,*]

[a] Department of Applied Mathematics and Statistics, Faculty of Sciences and Liberal Arts, Rajamangala University of Technology Isan, Nakhon Ratchasima, 30000, Thailand
[b] Department of Mathematics and Statistics, Hazara University, Mansehra, Pakistan
[c] Department of Mathematical Sciences, UAE University, P. O. Box, 15551, Al Ain, United Arab Emirates
[d] Department of Islamic Educational Management, Institute Agama Islam Negeri Curup, Rejang Lebong, Indonesia
[e] Mathematics Department, Al-Qunfudah University College, Umm Al-Qura University, Mecca, Saudi Arabia
[f] Faculty of Engineering and Technology, Future University, Cairo, Egypt

ARTICLE INFO

Keywords:
Mathematical robot system
Artificial intelligence
Particle swarm optimization
Active set procedure
Morlet wavelet
Numerical solutions

ABSTRACT

The task of this work is to present the solutions of the mathematical robot system (MRS) to examine the positive coronavirus cases through the artificial intelligence (AI) based Morlet wavelet neural network (MWNN). The MRS is divided into two classes, infected $I(\theta)$ and Robots $R(\theta)$. The design of the fitness function is presented by using the differential MRS and then optimized by the hybrid of the global swarming computational particle swarm optimization (PSO) and local active set procedure (ASP). For the exactness of the AI based MWNN-PSOIPS, the comparison of the results is presented by using the proposed and reference solutions. The reliability of the MWNN-PSOASP is authenticated by extending the data into 20 trials to check the performance of the scheme by using the statistical operators with 10 hidden numbers of neurons to solve the MRS.

1. Introduction

The prevalence of communicable diseases has long been a problem over the world. To name only few viruses, dengue fever (DF), which affects 2.5 billion people worldwide, is the most dangerous, contagious, and pandemic diseases. Due to ignorance and insufficient knowledge, DF is generally observed in the warmest areas in the world, such as South Asia [1,2]. There are deadly, contagious illnesses on every region of the planet, including HIV. HIV spreads like some of the other infections, and during the past few decades, numerous civilian casualties have been observed [3–5]. Lassa disease is a very severe illness that is primarily found in underdeveloped areas [6]. Malaria is another prevalent condition that transmits through indirect contact between hosts [7,8]. According to world health organization statistics, there have been claimed to have been one million cases from malaria, which primarily affects pregnant women and children from the United States and South Africa [9]. An additional contagious, fatal virus called Ebola is spread by people to infected animals [10]. The world has just been plagued by a deadly coronavirus epidemic that has had a negative impact on global economies, education sectors, sport events, tourism, business and airline sectors [11–13]. One human can infect another with the coronavirus [14]. Since the beginning of the coronavirus, it has abruptly halted people from living busy, rapid lives and has caused uncertainty throughout the entire planet. More deadly than before, it has now appeared in a wide variety of shapes, variants, and phases. It had an influence on the economies of numerous developed and emerging nations. Currently, one, two or three doses of various vaccines have been used throughout the world to begin the immunization process [15].

The majority of infections lack effective treatments or vaccines. Consequently, only a few medical safeguards have been approved to prevent the propagation of these infections. Because of this, the globe adopted several other precautions to prevent the spread of such infections, such as quarantines, social distances, handwashing, avoiding crowded areas, etc. One of the main causes of disease is free healthcare, which is provided by medical personnel such as doctors and nurses. A serious issue for the entire world is being caused by the rising number of positive coronavirus cases [16,17]. Numerous analytical/numerical approaches to the problem of infectious illnesses have been developed.

* Corresponding author.
E-mail addresses: sehazmi@uqu.edu.sa (S.E. Alhazmi), mohamed.reda@fue.edu.eg (M.R. Ali).

https://doi.org/10.1016/j.imu.2022.101081
Received 20 August 2022; Received in revised form 4 September 2022; Accepted 5 September 2022
Available online 24 September 2022

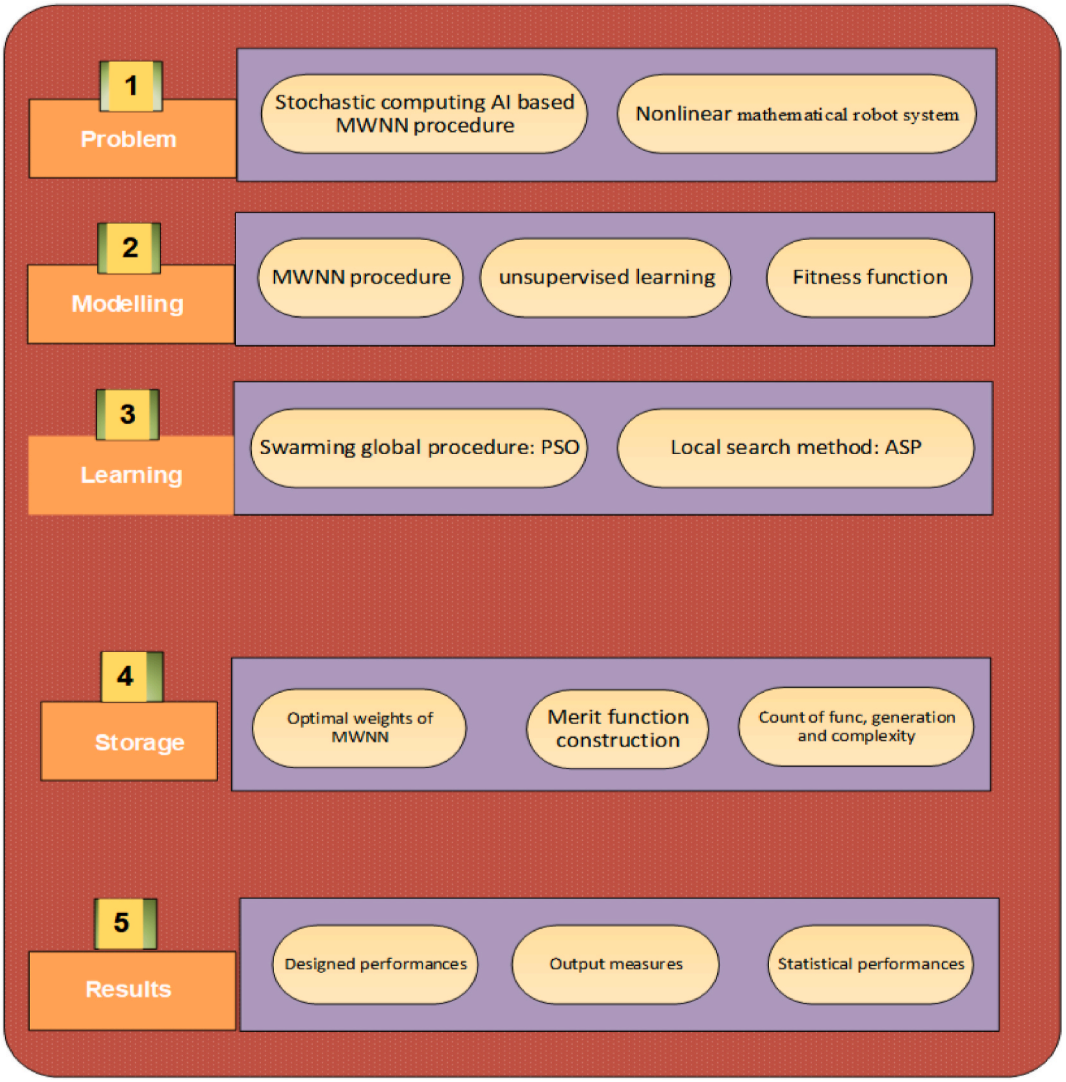

Fig. 1. Workflow illustration of MWNN-PSOASP for the MRS.

To mention some of them are Mickens employed a vaccination strategy based on distinct time to prevent the transmission of recurring viruses. Newton's embedded approach using the optimal control is applied by Ogren et al. [18] for the SIR dynamical system. The spatial measles outbreak was used on the fractional SIR epidemic by Goufo et al. [19]. Another few research projects based on infectious systems and theoretical advancements are given in these references [20–23]. Consequently, using robots to identify coronavirus-positive patients is crucial. The benefit of using robots is that they can provide medical assistance for those who are ill and stop the coronavirus spread. The dynamics of the MRS is divided into two classes, infected $I(\theta)$ and Robots $R(\theta)$, mathematically presented as [24]:

$$\begin{cases} I^{'}(\theta) = (a - bR(\theta) - u)I(\theta) + C(I), I_0 = i_1, \\ R^{'}(\theta) = c - dR(\theta), R_0 = i_2, \end{cases} \tag{1}$$

where $I(\theta)$ and $R(\theta)$ indicate the infected and Robot populations. a and c represent the newly infected individual and robot production rates. $C(I)$ is the migration factor using the human infected population, u shows the infected individual rate to death due to coronavirus, b is the detection rate based infected robots individual, d provides the stopping robot functioning rate, θ is the time, while i_1 and i_2 are the initial conditions (ICs).

The purpose of this study is to present the solutions of the mathematical robot system (MRS) to examine the positive coronavirus cases through the artificial intelligence (AI) based Morlet wavelet neural network (MWNN) under the optimization of the hybrid global swarming computational particle swarm optimization (PSO) and local active set procedure (ASP). The AI based stochastic solvers have been used in many applications, some of them are singular models [25,26], periodic differential models [27], food chain models [28–30] and economic/environmental models [31]. These presented stochastic based applications motivated the authors to explore the AI based MWNN-PSOIPS for solving the nonlinear MRS to achieve the stable and reliable numerical performances. Few of the novel features related to MWNN-PSOIPS are presented as:

- The solutions of the nonlinear MRS to examine the positive coronavirus cases using the AI based stochastic computing PSOIPS are presented.
- The stochastic AI based MWNN-PSOIPS is efficiently implemented to present the solutions of the nonlinear MRS.
- The exactness of the AI based MWNN-PSOIPS is obtained through the comparison of the proposed and reference results.
- The corroboration of AI based MWNN-PSOIPS is obtained using the statistical Theil inequality coefficient (TIC) and mean square error (MSE) to validate the dependability of the nonlinear MRS to examine the positive coronavirus cases.
- The absolute error (AE) is performed in good measures, which authenticates the accuracy of the MWNN-PSOIPS.

The remaining structure of the paper is presented as: Sect 2 presents the structure of the MWNN-PSOIPS. Sect 3 provides the comprehensive performances of the solutions. Sect 5 provides the conclusions along with upcoming reports.

2. Methodology

The current section presents the AI based MWNN-PSOIPS formulation to solve the MRS. Fig. 1 shows the graphical performances of the AI based MWNN-PSOIPS.

2.1. MWNN-PSOIPS design

The AI based MWNN-PSOIPS structure is presented to solve the MRS, which is shown in Eq. (1). The proposed solutions are represented as $\widehat{I}$ and $\widehat{R}$ with the derivatives of 1st kind is shown as:

$$[\widehat{I}(\theta),\widehat{R}(\theta)]=\left[\sum_{q=1}^{s}y_{I,q}N\left(\Psi_{I,q}\theta+z_{I,q}\right),\sum_{q=1}^{s}y_{R,q}N\left(\Psi_{R,q}\theta+z_{R,q}\right)\right], \tag{2}$$

$$[\widehat{I}^{'}(\theta),\widehat{R}^{'}(\theta)]=\left[\sum_{q=1}^{s}y_{I,q}N^{'}\left(\Psi_{I,q}\theta+z_{I,q}\right),\sum_{q=1}^{s}y_{R,q}N^{'}\left(\Psi_{R,q}\theta+z_{R,q}\right)\right],$$

where s presents the neurons and the unknown vectors $[\boldsymbol{y},\boldsymbol{\Psi},\boldsymbol{z}]$ are given as:

$\boldsymbol{W}=[\boldsymbol{W}_I,\boldsymbol{W}_R]$, for $\boldsymbol{W}_R=[\boldsymbol{y}_R,\boldsymbol{\Psi}_R,\boldsymbol{z}_R]$ and $\boldsymbol{W}_I=[\boldsymbol{y}_I,\boldsymbol{\Psi}_I,\boldsymbol{z}_I]$, where

$\boldsymbol{y}_I=\left[y_{I,1},y_{I,2},...,y_{I,s}\right],\boldsymbol{y}_R=\left[y_{R,1},y_{R,2},...,y_{R,s}\right],\boldsymbol{\Psi}_I=\left[\Psi_{I,1},\Psi_{I,2},...,\Psi_{I,s}\right]$, $\boldsymbol{\Psi}_R=\left[\Psi_{R,1},\Psi_{R,2},...,\Psi_{R,s}\right],\boldsymbol{z}_I=\left[z_{I,1},z_{I,2},...,z_{I,s}\right],\boldsymbol{z}_R=\left[z_{R,1},z_{R,2},...,z_{R,s}\right]$.

The AI based MWNN have been applied first time to solve the MRS. The Morlet function is mathematically depicted as:

$$N(\theta)=\cos(1.75\theta)\exp\left(-\frac{1}{2}\theta^2\right), \tag{3}$$

Eq. (2) is updated as:

$$[\widehat{I}(\theta),\widehat{R}(\theta)]=\begin{bmatrix}\sum_{q=1}^{s}y_{I,q}\cos\left(1.75\left(\Psi_{I,q}\theta+z_{I,q}\right)\right)e^{-0.5\left(\Psi_{I,q}\theta+z_{I,q}\right)^2},\\ \sum_{q=1}^{s}y_{R,q}\cos\left(1.75\left(\Psi_{R,q}\theta+z_{R,q}\right)\right)e^{-0.5\left(\Psi_{R,q}\theta+z_{IRq}\right)^2}\end{bmatrix}, \tag{4}$$

$$[\widehat{I}^{'}(\theta),\widehat{R}^{'}(\theta)]=\left[\sum_{q=1}^{s}2y_{I,q}\Psi_{I,q}\left(\frac{e^{\left(\Psi_{I,q}\theta+z_{I,q}\right)}}{1+\left(e^{\left(\Psi_{I,q}\theta+z_{I,q}\right)}\right)^2}\right),\sum_{q=1}^{s}2y_{R,q}\Psi_{R,q}\left(\frac{e^{\left(\Psi_{R,q}\theta+z_{R,q}\right)}}{1+\left(e^{\left(\Psi_{R,q}\theta+z_{R,q}\right)}\right)^2}\right)\right],$$

To present the solution of the MRS, a merit function is presented as:

$$M_F=M_{F-1}+M_{F-2}+M_{F-3}, \tag{5}$$

where, M_{F-1} and M_{F-2} are the merit functions using the infected and Robot population, $I(\theta)$ and $R(\theta)$ that are constructed using the different MRS, while the construction of M_{F-3} is based on the ICs of the MRS, shown as:

$$M_{F-1}=\frac{1}{N}\sum_{q=1}^{K}\left(\widehat{I}_q^{'}-\left(a-b\widehat{R}_q-u\right)\widehat{I}_q-C\left(\widehat{I}_q\right)\right)^2, \tag{6}$$

$$M_{F-2}=\frac{1}{N}\sum_{q=1}^{K}\left(\widehat{R}_q^{'}+d\widehat{R}_q-c\right)^2, \tag{7}$$

$$M_{F-3}=\frac{1}{2}\left((\widehat{I}_0-i_1)^2+(\widehat{R}_0-i_2)^2\right), \tag{8}$$

$$Kh=1,\widehat{I}_q=\widehat{I}(\theta_q),\widehat{R}_q=\widehat{R}(\theta_q),\theta_q=qh.$$

2.2. Optimization: PSOASP

The current section shows the procedure of optimization using the PSOASP to solve the MRS. Fig. 1 shows the workflow illustrations based on the MWNN-PSOASP for the MRS.

The method for computationally optimizing global search swarming approach called PSO is used to substitute the genetic algorithms. The PSO technique was first established during the last decade by Kennedy and Eberhart [32]. PSO displays the outcomes of multiple intricate systems that manage a specific population utilizing the technique of optimum training. PSO can be completed easily due to the minimal storage capacity [33]. In recent decades, PSO is used in various submissions, e.g., engineering systems [34], multi-objective multimodal methods [35], solar energy models [36], cataloguing the photovoltaic based single/double/triple parameter diode [37], plant diseases [38], image organization [39], particle filter noise reduction based on the analysis of mechanical accountability [30] and green coal production networks [40]. These submissions stimulated the authors to perform the swarming approaches for the MRS.

A local search optimization technique known as active set programming is used to improve the performance of unconstrained and convex models. Recently, ASP is applied in various applications, some of

them are realizable safety critical control [41], linearly non-lipschitz constrained nonconvex optimization [42], lung tumor detection and classification [43], atrial fibrillation detection based on transfer learning [44], characterizations of discrete-time descriptor systems [45], pressure-dependent models of water distribution systems [46] and embedded model predictive control [47]. The AI based MWNN-PSOASP is implemented to present the numerical solutions of the MRS. Fig. 1 shows the workflow illustration of MWNN-PSOASP for the MRS.

The pseudocode of the current study based on the optimization procedure to solve the MRS is presented below as:

Pseudocode using the MWNN-PSOASP for the MRS.

Pseudocode using the MWNN-PSOASP for the MRS

PSO starts

Inputs: The values of the chromosomes $\boldsymbol{W}=[\boldsymbol{W}_I,\boldsymbol{W}_R]$, for $\boldsymbol{W}_R=[\boldsymbol{y}_R,\boldsymbol{\Psi}_R,\boldsymbol{z}_R]$ and $\boldsymbol{W}_I=[\boldsymbol{y}_I,\boldsymbol{\Psi}_I,\boldsymbol{z}_I]$.

Population: The chromosomes for the q^{th} variables are $\boldsymbol{y}_I=[y_{I,1},y_{I,2},...,y_{I,s}]$, $\boldsymbol{y}_R=[y_{R,1},y_{R,2},...,y_{R,s}]$, $\boldsymbol{\Psi}_I=[\Psi_{I,1},\Psi_{I,2},...,\Psi_{I,s}]$, $\boldsymbol{\Psi}_R=[\Psi_{R,1},\Psi_{R,2},...,\Psi_{R,s}]$, $\boldsymbol{z}_I=[z_{I,1},z_{I,2},...,z_{I,s}]$, $\boldsymbol{z}_R=[z_{R,1},z_{R,2},...,z_{R,s}]$.

Output: The optimal swarming measures are $\boldsymbol{W}_{\mathbf{B.PSO}}$

Initialization: Construct the weight matrix ($\boldsymbol{W}$) for the performances of the real bounds to elect the chromosome. $\boldsymbol{W}$ shows the initial population. Indicate the primary random swarm to set the PSO and 'gaoptimset'.

Fitness Evaluation: Obtain the M_F by using the Eqs (5) to (8).

Stopping criteria: Terminate if TolFun $=10^{-19}$, population span = (-15,15), Initial weights= decreasing, particlesize = 55, HybridFcn =@fmincon, SwarmSize=100, velocity span = (-3,3), then Go to [**storage**].

Ranking: Present the Rank "$\boldsymbol{W}$" using the "$\boldsymbol{P}$" based on the M_F.

Storage: $\boldsymbol{W}_{\mathbf{B.PSO}}$ presents the optimal weights, M_F, complexity, generations and count of function using the execution of PSO.

Swarming optimization procedure Ends

ASP starts

Inputs: $\boldsymbol{W}_{\mathbf{B.\ PSO}}$

Output: The Optimal measures using PSOASP are $\boldsymbol{W}_{\boldsymbol{PSOASP}}$

Initialize: Regulate the generations, constrains and other performances.

Dismiss: ASP stops, when the values of the generations are 740, $M_F = 10^{-20}$, MaxFunEvals = 275000, and TolFun/Con/X=10^{-19} obtained.

Fitness: M_F for each $\boldsymbol{W}$ based population $\boldsymbol{P}$ for (5) to (8).

Modifications: Fmincon of the ASP for the fine-tune of $\boldsymbol{W}$.

Accumulate: M_F, $\boldsymbol{W}_{\mathbf{B.\ PSO}}$, epochs, time, and count of function.

ASP ends

2.3. Statistical performances

The current section shows the mathematical performances based on the TIC and MSE for solving the MRS, which is shown as:

$$\left[\mathrm{TIC}_I,\mathrm{TIC}_R\right]=\left(\frac{\sqrt{\frac{1}{n}\sum_{q=1}^{n}\left(I_q-\widehat{I}_q\right)^2}}{\left(\sqrt{\frac{1}{n}\sum_{q=1}^{n}I_q^2}+\sqrt{\frac{1}{n}\sum_{q=1}^{n}\widehat{I}_q^2}\right)},\frac{\sqrt{\frac{1}{n}\sum_{q=1}^{n}\left(R_q-\widehat{R}_q\right)^2}}{\left(\sqrt{\frac{1}{n}\sum_{q=1}^{n}R_q^2}+\sqrt{\frac{1}{n}\sum_{q=1}^{n}\widehat{R}_q^2}\right)}\right), \tag{9}$$

$$\left[\mathrm{MSE}_I,\mathrm{MSE}_R\right]=\left[\sum_{q=1}^{n}\left(I_q-\widehat{I}_q\right)^2,\sum_{q=1}^{n}\left(R_q-\widehat{R}_q\right)^2\right]. \tag{10}$$

3. Simulation and results

This section indicated the numerical simulations based on the AI based MWNN-PSOASP for the MRS. The comparison performances based on the reference and obtained results are presented to authenticate the consistency of the procedure. Consider $d=0.2$, $c=0.1$, $C(I)=C=2$, $b=0.1$, $a=0.5$, $u=0.3$, $i_1=0.6$ and $i_2=0.5$ are presented as:

$$\begin{cases} I'(\theta)=(0.5-0.1R(\theta)-0.3)I(\theta)+2, I_0=0.5, \\ R'(\theta)=0.1-0.2R(\theta), R_0=0.6. \end{cases}$$

A M_F takes the form as:

$$M_F=\frac{1}{N}\sum_{q=1}^{K}\left(\left(\widehat{I}_q'-0.5\widehat{I}_q+0.1\widehat{R}_q\widehat{I}_q+0.3\widehat{I}_q+2\right)^2+\left(\widehat{R}_q'-0.1+0.2\widehat{R}_q\right)^2\right)+\frac{1}{2}\left((\widehat{I}_0-0.5)^2+(\widehat{R}_0-0.6)^2\right) \tag{12}$$

The optimization performances using the AI based MWNN-PSOASP for the MRS are provided for twenty independent trials to perform the parameter of the model. The values of the numerical outputs have been achieved in the [0, 1] with the step size 0.05. The proposed values of the $I(\theta)$ and $R(\theta)$ are shown as:

$$\begin{aligned}\widehat{I}(\theta) = {} & 3.41\cos\left(\frac{4}{3}(0.61\theta-2.48)\right)e^{-\frac{1}{2}(0.61\theta-2.48)^2}+0.56\cos\left(\frac{4}{3}(1.58\theta+0.97)\right)e^{-\frac{1}{2}(1.58\theta+0.97)^2}\\ & -0.57\cos\left(\frac{4}{3}(1.42\theta+2.34)\right)e^{-\frac{1}{2}(1.42\theta+2.34)^2}+1.16\cos\left(\frac{4}{3}(0.61\theta+0.68)\right)e^{-\frac{1}{2}(0.61\theta+0.68)^2}\\ & +2.24\cos\left(\frac{4}{3}(1.12\theta+2.75)\right)e^{-\frac{1}{2}(1.12\theta+2.75)^2}-0.31\cos\left(\frac{4}{3}(0.98\theta+1.89)\right)e^{-\frac{1}{2}(0.98\theta+1.89)^2}\\ & -1.29\cos\left(\frac{4}{3}(1.48\theta+1.34)\right)e^{-\frac{1}{2}(1.48\theta+1.34)^2}-2.83\cos\left(\frac{4}{3}(-0.1\theta+0.25)\right)e^{-\frac{1}{2}(-0.1\theta+0.25)^2}\\ & -2.27\cos\left(\frac{4}{3}(-0.4\theta+0.71)\right)e^{-\frac{1}{2}(-0.4\theta+0.71)^2}+3.61\cos\left(\frac{4}{3}(2.50\theta+4.80)\right)e^{-\frac{1}{2}(2.50\theta+4.80)^2},\end{aligned} \tag{13}$$

$$\begin{aligned}\widehat{R}(\theta) = {} & -0.1\cos\left(\frac{4}{3}(0.18\theta+0.55)\right)e^{-\frac{1}{2}(0.18\theta+0.55)^2}+0.26\cos\left(\frac{4}{3}(0.18\theta+1.24)\right)e^{-\frac{1}{2}(0.18\theta+1.24)^2}\\ & +0.14\cos\left(\frac{4}{3}(-0.08\theta-0.5)\right)e^{-\frac{1}{2}(-0.08\theta-0.5)^2}+0.61\cos\left(\frac{4}{3}(0.20\theta+2.01)\right)e^{-\frac{1}{2}(0.20\theta+2.01)^2}\\ & +0.05\cos\left(\frac{4}{3}(-0.2\theta+0.09)\right)e^{-\frac{1}{2}(-0.2\theta+0.09)^2}+0.03\cos\left(\frac{4}{3}(-0.7\theta-1.70)\right)e^{-\frac{1}{2}(-0.7\theta-1.70)^2}\\ & -0.008\cos\left(\frac{4}{3}(0.3\theta+0.030)\right)e^{-\frac{1}{2}(0.3\theta+0.03)^2}+0.34\cos\left(\frac{4}{3}(-0.1\theta-0.78)\right)e^{-\frac{1}{2}(-0.1\theta-0.78)^2}\\ & +0.2\cos\left(\frac{4}{3}(0.02\theta-0.098)\right)e^{-\frac{1}{2}(0.02\theta-0.09)^2}-0.15\cos\left(\frac{4}{3}(-0.1\theta+0.06)\right)e^{-\frac{1}{2}(-0.1\theta+0.06)^2},\end{aligned} \tag{14}$$

Figs. 3 and 4 indicates the statistical performances of the $I(\theta)$ and $R(\theta)$ for the MRS. The Mean, Maximum (Max), standard deviation (STD), Median (MD), Minimum (Min), and Semi-interquartile range (SIR) for the MRS are presented in Table 1 and Table 2. The mathematical performance of the SIR is the difference of ½ times of quartile 3rd and 1st. The Mean, STD, MD and SIR performances have been performed for both $I(\theta)$ and $R(\theta)$ of the MRS are 10^{-06} to 10^{-07}. The Max values shows the poor results but found as 10^{-05} to 10^{-06} for both $I(\theta)$ and $R(\theta)$. The Min performances shows the good results, which are found for both classes are 10^{-07} to 10^{-11}. These calculated operator small measures represent the dependability of the AI based on the MWNN-PSOASP for the MRS.

Fig. 2 presents the optimal weights and result comparison for $I(\theta)$ and $R(\theta)$ of the MRS. The optimal weight vectors are illustrated plotted in Fig. 2(a and b) for the MRS, while the results are performed in Fig. 2(c and d) of the MRS. These overlapping of the mean, best and worst solutions is performed to check the correctness of the AI based MWNNs-PSOASP. Fig. 2(e) provides the AE performances for $I(\theta)$ and $R(\theta)$ of the MRS. For the $I(\theta)$ and $R(\theta)$ categories of the MRS, the AE measures are performed around 10^{-06} to 10^{-08} and 10^{-07} to 10^{-08}. These calculated optimal performances based on the AE represent the exactness of the AI based MWNN-PSOASP.

Fig. 3 presents the statistical computing measures for the $I(\theta)$ and $R(\theta)$ classes of the MRS. The statistical TIC and MSE operators have been used to present the numerical solutions of the MRS. One can observe that the TIC values for $I(\theta)$ and $R(\theta)$ classes of the MRS are measured as 10^{-10}-10^{-11} and 10^{-11}-10^{-12}. The MSE operator values for both the classes $I(\theta)$ and $R(\theta)$ lie as 10^{-13}-10^{-14}. These performances indicate the correctness of the AI based MWNN-PSOASP for the MRS.

To check the consistency of the AI based MWNN-PSOASP for the MRS, the statistical TIC and MSE interpretations have been illustrated in Fig. 4-6. Twenty trials have been implemented in input domain [0,1] by taking 10 number of neurons. The TIC convergence values have been plotted as 10^{-09}-10^{-10} and 10^{-10}-10^{-11} for $I(\theta)$ and $R(\theta)$. Similarly, MSE convergence performances have been derived as 10^{-11}-10^{-13} and 10^{-12}-10^{-13} for $I(\theta)$ and $R(\theta)$ of the MRS. These optimal performances using the AI based MWNN-PSOASP authenticate that the proposed scheme performs well to solve the MRS (see Fig. 5).

4. Concluding remarks

The purpose of these investigations is to present the numerical solutions of the mathematical robot system to examine the positive coronavirus cases. The design of the artificial intelligence-based Morlet wavelet neural network has been presented first time to solve the mathematical robot system. The mathematical robot system has been categorized into two dynamics, infected $I(\theta)$ and Robots $R(\theta)$. Few concluding remarks of this study are presented as:

- The design of the AI based MWNN along with the optimization efficiency of PSOASM is presented first time to solve the mathematical robot system.
- The proposed AI based MWNN-PSOAPS is effectively applied to solve the mathematical robot system.
- For the exactness of the AI based MWNN-PSOIPS, the comparison of the results has been presented by using the proposed and reference solutions.
- The reliability of the MWNN-PSOASP has been authenticated by extending the data into 20 trials to check the performance of the

Table 1
Statistical operator performances for.$I(\theta)$

θ	$I(\alpha)$					
	Mean	Max	STD	MD	Min	SIR
0	4.54674E-07	4.90402E-06	1.07541E-06	1.75826E-07	7.10649E-11	2.39063E-07
0.05	8.50202E-07	6.91587E-06	1.50625E-06	4.09634E-07	5.03369E-09	2.34732E-07
0.1	1.43577E-06	6.75494E-06	1.59467E-06	9.45636E-07	9.66264E-08	6.37282E-07
0.15	2.50968E-06	1.03194E-05	2.36168E-06	1.92842E-06	1.04942E-07	1.25302E-06
0.2	3.21751E-06	1.37793E-05	3.14077E-06	2.85585E-06	1.52113E-07	2.02217E-06
0.25	3.31684E-06	1.42339E-05	3.39703E-06	2.66063E-06	1.81681E-08	2.22107E-06
0.3	2.85017E-06	1.21896E-05	3.13704E-06	2.27382E-06	5.16728E-08	1.86375E-06
0.35	2.15496E-06	9.03015E-06	2.47878E-06	1.52121E-06	1.43166E-08	9.39160E-07
0.4	1.31191E-06	7.96198E-06	1.90939E-06	6.86554E-07	1.83868E-08	3.92892E-07
0.45	1.03345E-06	5.92670E-06	1.41285E-06	4.92309E-07	4.13522E-08	5.37661E-07
0.5	1.24158E-06	4.48179E-06	1.12813E-06	8.96362E-07	4.58559E-08	6.35915E-07
0.55	1.19577E-06	6.83674E-06	1.41559E-06	8.39599E-07	2.50308E-07	4.55329E-07
0.6	1.17749E-06	9.10337E-06	1.95084E-06	7.05512E-07	8.88368E-09	5.74924E-07
0.65	1.91972E-06	1.08727E-05	2.35191E-06	1.36164E-06	5.64084E-08	7.46043E-07
0.7	2.77014E-06	1.17677E-05	2.78416E-06	2.18574E-06	1.41055E-07	1.38304E-06
0.75	3.40234E-06	1.15413E-05	3.05703E-06	2.72830E-06	3.46908E-08	2.05816E-06
0.8	3.48297E-06	1.08901E-05	3.06579E-06	2.72537E-06	3.80029E-07	2.16012E-06
0.85	3.02570E-06	1.06894E-05	2.65767E-06	2.49113E-06	3.94092E-07	1.68071E-06
0.9	2.14565E-06	9.15875E-06	2.30348E-06	1.42499E-06	8.90565E-08	8.20232E-07
0.95	1.61955E-06	7.63815E-06	2.31111E-06	6.39825E-07	1.01675E-07	4.31817E-07
1	1.60816E-06	7.03658E-06	2.24844E-06	6.89440E-07	3.11178E-08	6.28636E-07

Table 2
Statistical operator performances for.$R(\theta)$

θ	$R(\theta)$					
	Mean	Max	STD	MD	Min	SIR
0	6.99460E-07	4.08335E-06	1.18329E-06	1.28407E-07	4.52558E-11	4.59012E-07
0.05	1.02726E-06	4.77161E-06	1.19940E-06	6.79014E-07	6.14489E-08	4.07815E-07
0.1	1.10895E-06	4.73802E-06	1.41447E-06	4.51034E-07	2.76715E-08	7.40714E-07
0.15	1.43775E-06	5.26152E-06	1.58219E-06	5.56007E-07	1.35583E-07	1.31568E-06
0.2	1.69645E-06	5.42398E-06	1.62995E-06	1.06686E-06	5.07068E-08	1.32827E-06
0.25	1.77104E-06	6.39889E-06	1.64773E-06	1.51742E-06	3.35034E-08	8.96608E-07
0.3	1.65634E-06	6.34479E-06	1.67096E-06	1.48981E-06	1.95450E-08	7.47756E-07
0.35	1.58544E-06	5.54289E-06	1.41214E-06	9.79522E-07	2.67251E-07	8.58269E-07
0.4	1.37958E-06	4.31668E-06	1.08515E-06	9.64483E-07	2.94522E-07	7.07770E-07
0.45	1.09051E-06	2.93435E-06	8.50722E-07	9.42918E-07	6.43934E-08	5.79809E-07
0.5	9.11132E-07	2.70075E-06	8.70778E-07	5.39011E-07	4.37776E-08	7.04615E-07
0.55	1.01544E-06	3.27748E-06	1.07882E-06	5.01748E-07	5.62508E-09	8.23989E-07
0.6	1.37673E-06	4.22142E-06	1.17568E-06	1.05988E-06	1.34298E-09	7.02332E-07
0.65	1.56921E-06	4.66951E-06	1.30563E-06	1.27681E-06	7.53043E-08	8.68021E-07
0.7	1.51554E-06	5.42980E-06	1.40851E-06	1.23761E-06	9.53281E-08	8.49305E-07
0.75	1.31311E-06	5.90948E-06	1.37913E-06	8.22917E-07	3.31786E-08	6.87327E-07
0.8	1.09372E-06	6.05496E-06	1.39529E-06	4.67729E-07	1.63426E-08	6.48860E-07
0.85	1.32931E-06	5.86506E-06	1.46699E-06	8.17396E-07	6.71198E-09	9.54506E-07
0.9	1.68167E-06	5.93889E-06	1.69677E-06	9.63803E-07	3.03388E-07	9.65987E-07
0.95	1.74649E-06	6.86096E-06	1.77784E-06	1.03184E-06	1.67538E-07	9.49239E-07
1	1.28010E-06	4.67303E-06	1.33233E-06	9.98536E-07	5.68242E-08	6.78837E-07

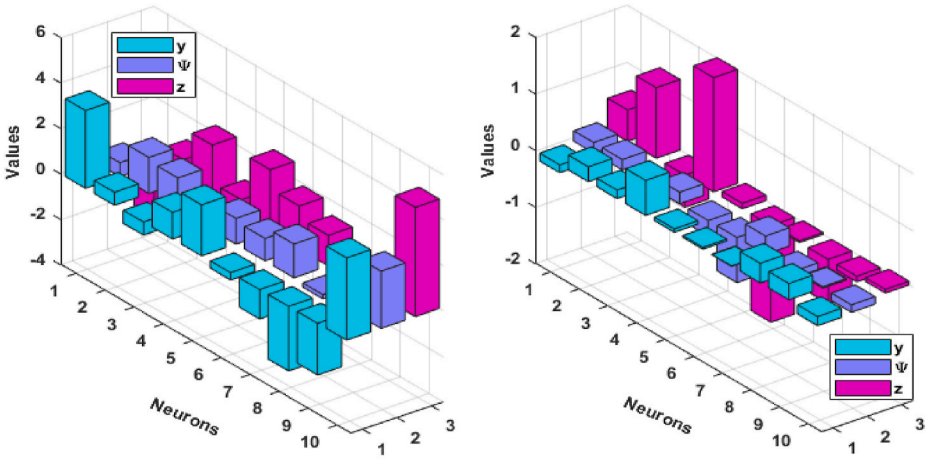

(a) Weights: $I(\theta)$ (b) Weights: $R(\theta)$

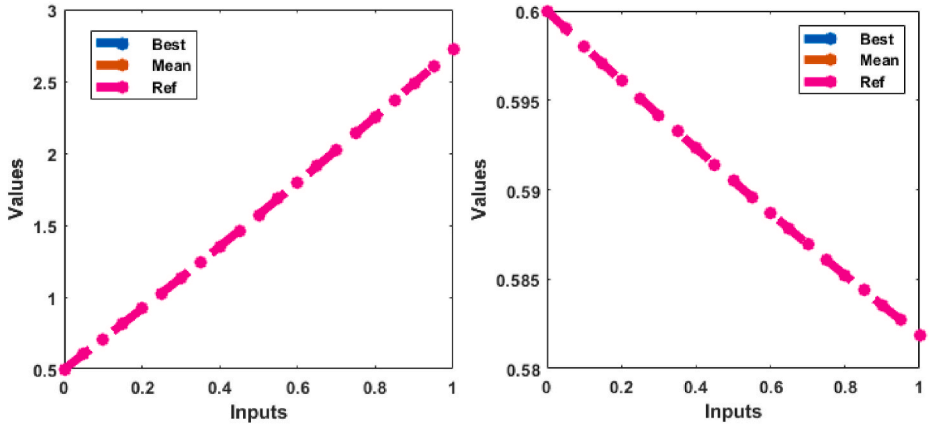

(c) Comparison: $I(\theta)$ (d) Comparison: $R(\theta)$

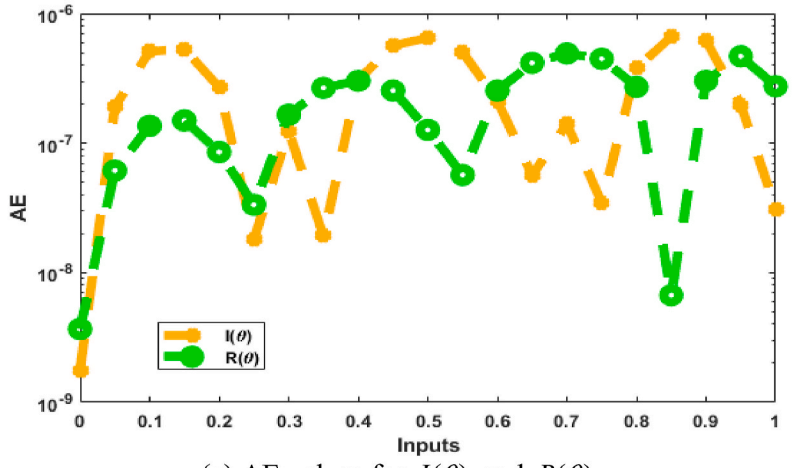

(e) AE values for $I(\theta)$ and $R(\theta)$

Fig. 2. Optimal weights, comparison performances and AE for $I(\theta)$ and $R(\theta)$ of the MRS.

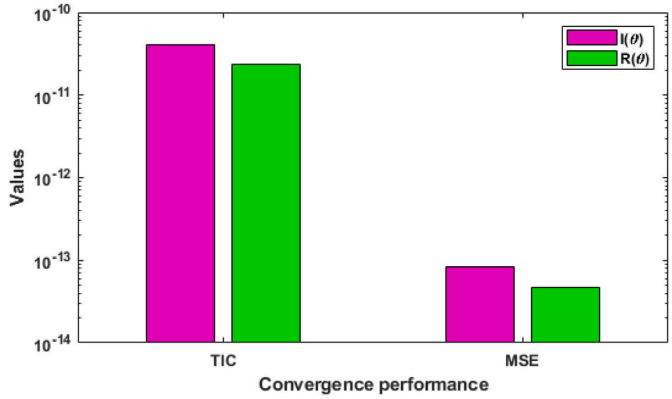

Fig. 3. Performances of the statistical operators for $I(\theta)$ and $R(\theta)$ of the MRS.

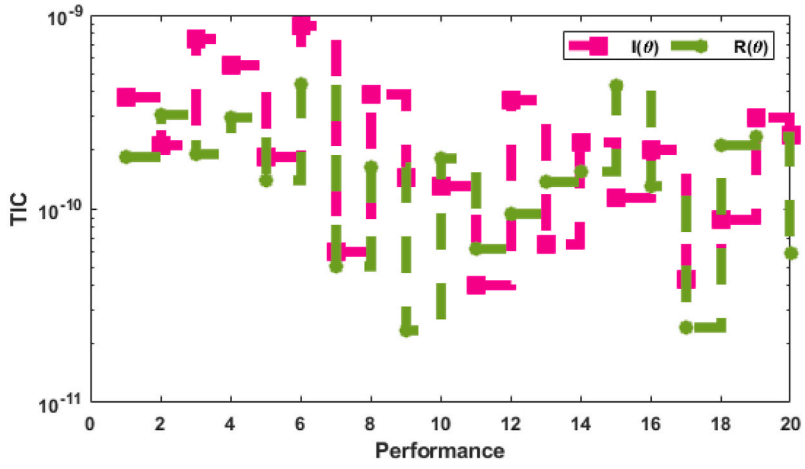

TIC operator measures for $I(\theta)$ and $R(\theta)$

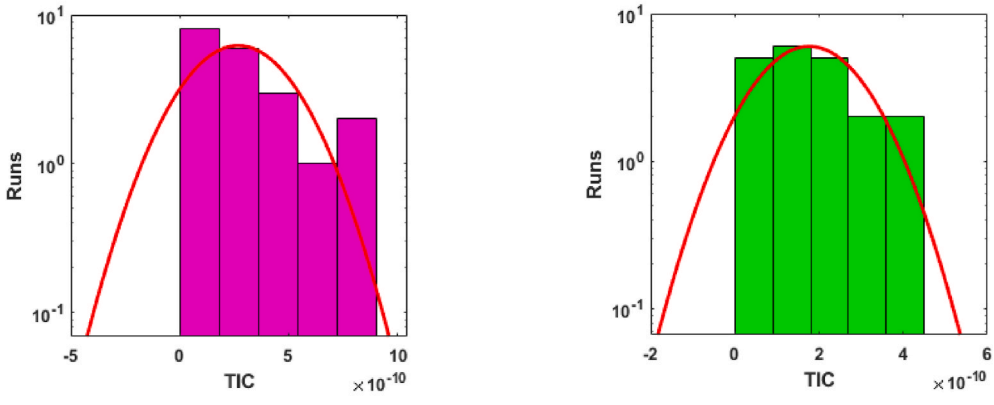

(a) HG: $I(\theta)$ **(b)** HG: $R(\theta)$

Fig. 4. TIC operator convergence measures performances for $I(\theta)$ and $R(\theta)$ of the MRS.

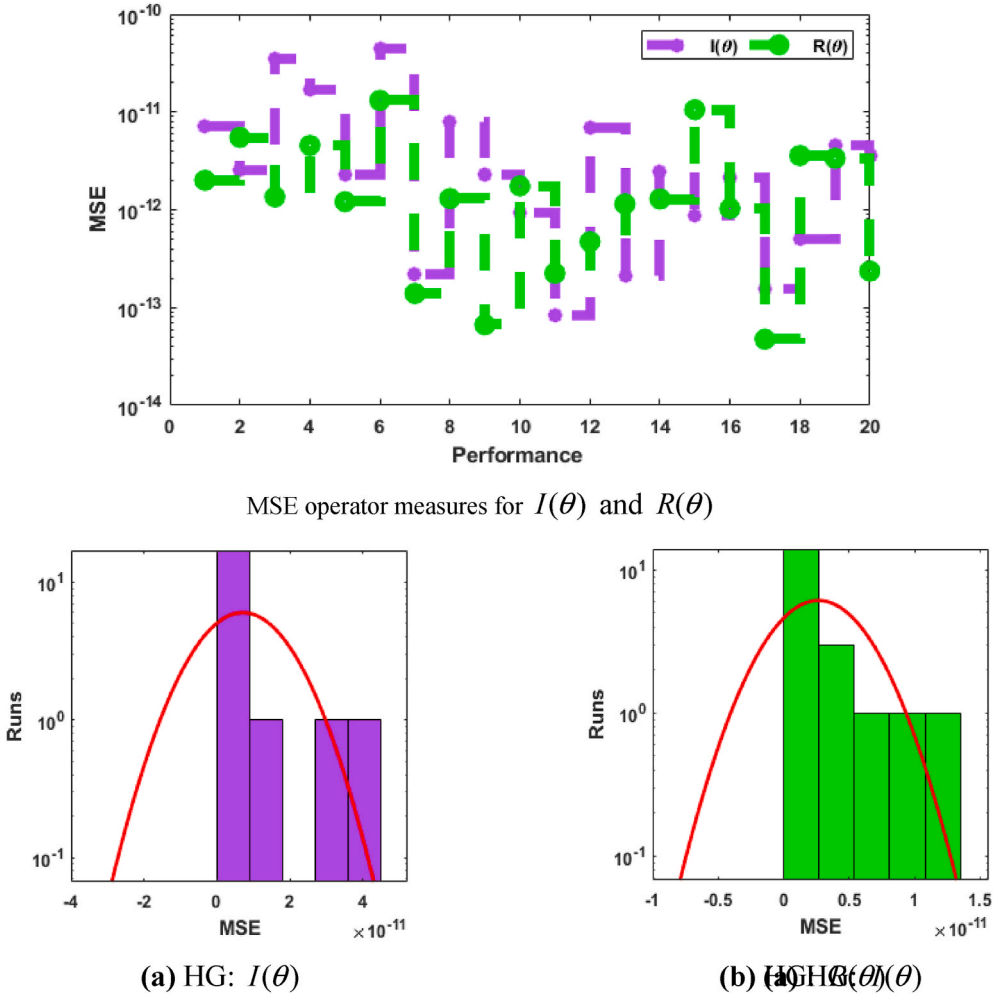

Fig. 5. MSE operator convergence measures performances for $I(\theta)$ and $R(\theta)$ of the MRS.

scheme through the statistical operators with 10 hidden numbers of neurons to solve the MRS.

Future research directions

The proposed AI based MWNN-PSOASP can be implemented to solve various nonlinear, fractional and fluid dynamic systems [48–54].

Declaration of competing interest

The authors declare that they have no known competing financial interests or personal relationships that could have appeared to influence the work reported in this paper.

Acknowledgement

The authors would like to thank the Deanship of Scientific Research at Umm Al-Qura University for supporting this work by Grant Code: (22UQU4282396DSR19).

References

[1] Side S, Noorani MSM. A SIR model for spread of dengue fever disease (simulation for South Sulawesi, Indonesia and Selangor, Malaysia). World J Model Simulat 2013;9(2):96–105.
[2] Bhatt S, Gething PW, Brady OJ, Messina JP, Farlow AW, Moyes CL, Drake JM, Brownstein JS, Hoen AG, Sankoh O, Myers MF. The global distribution and burden of dengue. Nature 2013;496(7446):504–7.
[3] Guerrero–Sánchez Y, Umar M, Sabir Z, Guirao JL, Raja MAZ. Solving a class of biological HIV infection model of latently infected cells using heuristic approach. Discrete & Continuous Dynamical Systems-S 2021;14(10):3611.
[4] Umar M, Sabir Z, Amin F, Guirao JL, Raja MAZ. Stochastic numerical technique for solving HIV infection model of CD4+ T cells. The European Physical Journal Plus 2020;135(5):1–19.
[5] Umar M, Sabir Z, Raja MAZ, Aguilar JG, Amin F, Shoaib M. Neuro-swarm intelligent computing paradigm for nonlinear HIV infection model with CD4+ T-cells. Math Comput Simulat 2021;188:241–53.
[6] McCormick JB, King IJ, Webb PA, Johnson KM, O'Sullivan R, Smith ES, Trippel S, Tong TC. A case-control study of the clinical diagnosis and course of Lassa fever. JID (J Infect Dis) 1987;155(3):445–55.
[7] Bushman M, Antia R, Udhayakumar V, de Roode JC. Within-host competition can delay evolution of drug resistance in malaria. PLoS Biol 2018;16(8):e2005712.
[8] Smith DG, Ferrell RE. A family study of the hemoglobin polymorphism in Macaca fascicularis. J Hum Evol 1980;9(7):557–63.
[9] Kakuru A, Staedke SG, Dorsey G, Rogerson S, Chandramohan D. Impact of Plasmodium falciparum malaria and intermittent preventive treatment of malaria in pregnancy on the risk of malaria in infants: a systematic review. Malar J 2019;18(1):1–13.
[10] Emond RT, Evans B, Bowen ET, Lloyd G. A case of Ebola virus infection. Br Med J 1977;2(6086):541–4.
[11] Umar M, Sabir Z, Raja MAZ, Shoaib M, Gupta M, Sánchez YG. A stochastic intelligent computing with neuro-evolution heuristics for nonlinear SITR system of novel COVID-19 dynamics. Symmetry 2020;12(10):1628.
[12] Umar M, Sabir Z, Raja MAZ, Amin F, Saeed T, Guerrero-Sanchez Y. Integrated neuro-swarm heuristic with interior-point for nonlinear SITR model for dynamics of novel COVID-19. Alex Eng J 2021;60(3):2811–24.
[13] Sánchez YG, Sabir Z, Guirao JL. Design of a nonlinear SITR fractal model based on the dynamics of a novel coronavirus (COVID-19). Fractals 2020;28(8):2040026.
[14] Redhwan SS, Abdo MS, Shah K, Abdeljawad T, Dawood S, Abdo HA, Shaikh SL. Mathematical modeling for the outbreak of the coronavirus (COVID-19) under fractional nonlocal operator. Results Phys 2020;19:103610.

[15] Gao W, Baskonus HM, Shi L. New investigation of bats-hosts-reservoir-people coronavirus model and application to 2019-nCoV system. Adv Differ Equ 2020; 2020(1):1–11.
[16] Thabet ST, Abdo MS, Shah K. Theoretical and numerical analysis for transmission dynamics of COVID-19 mathematical model involving Caputo–Fabrizio derivative. Adv Differ Equ 2021;2021(1):1–17.
[17] Jeelani MB, Alnahdi AS, Abdo MS, Abdulwasaa MA, Shah K, Wahash HA. Mathematical modeling and forecasting of COVID-19 in Saudi arabia under fractal-fractional derivative in caputo sense with power-law. Axioms 2021;10(3):228.
[18] Ögren P, Martin CF. Vaccination strategies for epidemics in highly mobile populations. Appl Math Comput 2002;127(2–3):261–76.
[19] Goufo D, Franc E, OukouomiNoutchie SC, Mugisha S. A fractional SEIR epidemic model for spatial and temporal spread of measles in metapopulations. In: Abstract and applied analysis, vol. 2014. Hindawi; 2014.
[20] Dietz K. The first epidemic model: a historical note on PD En'ko. Aust J Stat 1988; 30(1):56–65.
[21] Hethcote HW. The mathematics of infectious diseases. SIAM Rev 2000;42(4): 599–653.
[22] Botmart T, Sabir Z, Raja MAZ, Weera W, Sadat R, Ali MR. A numerical study of the fractional order dynamical nonlinear susceptible infected and quarantine differential model using the stochastic numerical approach. Fractal and Fractional 2022;6(3):139.
[23] Wickwire K. Mathematical models for the control of pests and infectious diseases: a survey. Theor Popul Biol 1977;11(2):182–238.
[24] Zhang H, Jiao J, Chen L. Pest management through continuous and impulsive control strategies. Biosystems 2007;90(2):350–61.
[25] Baba IA, Baba BA, Esmaili P. A mathematical model to study the effectiveness of some of the strategies adopted in curtailing the spread of COVID-19. Comput Math Methods Med 2020. 2020.
[26] Sabir Z, Raja MAZ, Guirao JL, Shoaib M. Integrated intelligent computing with neuro-swarming solver for multi-singular fourth-order nonlinear Emden–Fowler equation. Comput Appl Math 2020;39(4):1–18.
[27] Sabir Z, Wahab HA, Javeed S, Baskonus HM. An efficient stochastic numerical computing framework for the nonlinear higher order singular models. Fractal and Fractional 2021;5(4):176.
[28] Sabir Z, Khalique CM, Raja MAZ, Baleanu D. Evolutionary computing for nonlinear singular boundary value problems using neural network, genetic algorithm and active-set algorithm. The European Physical Journal Plus 2021;136(2):1–19.
[29] Sabir Z. Stochastic numerical investigations for nonlinear three-species food chain system. Int J Biomath (IJB) 2022;15(4):2250005.
[30] Souayeh B, Sabir Z, Umar M, Alam MW. Supervised neural network procedures for the novel fractional food supply model. Fractal and Fractional 2022;6(6):333.
[31] Sabir Z, Ali MR, Sadat R. Gudermannian neural networks using the optimization procedures of genetic algorithm and active set approach for the three-species food chain nonlinear model. J Ambient Intell Hum Comput 2022:1–10.
[32] Kiani AK, Khan WU, Raja MAZ, He Y, Sabir Z, Shoaib M. Intelligent backpropagation networks with bayesian regularization for mathematical models of environmental economic systems. Sustainability 2021;13(17):9537.
[33] Shi Y, Eberhart RC. Empirical study of particle swarm optimization. In: Proceedings of the 1999 congress on evolutionary computation-CEC99, vol. 3. IEEE; 1999. p. 1945–50.
[34] Engelbrecht AP. Computational intelligence: an introduction. second ed. Chichester, U.K.: John Wiley & Sons Ltd.; 2007.
[35] De Almeida BSG, Leite VC. Particle swarm optimization: a powerful technique for solving engineering problems. Swarm intelligence-recent advances, new perspectives and applications. 2019. p. 1–21.
[36] Zhang X, Liu H, Tu L. A modified particle swarm optimization for multimodal multi-objective optimization. Eng Appl Artif Intell 2020;95:103905.
[37] Elsheikh AH, Abd Elaziz M. Review on applications of particle swarm optimization in solar energy systems. Int J Environ Sci Technol 2019;16(2):1159–70.
[38] Yousri D, Thanikanti SB, Allam D, Ramachandaramurthy VK, Eteiba MB. Fractional chaotic ensemble particle swarm optimizer for identifying the single, double, and three diode photovoltaic models' parameters. Energy 2020;195:116979.
[39] Darwish A, Ezzat D, Hassanien AE. An optimized model based on convolutional neural networks and orthogonal learning particle swarm optimization algorithm for plant diseases diagnosis. Swarm Evol Comput 2020;52:100616.
[40] Chen H, Fan DL, Fang L, Huang W, Huang J, Cao C, Yang L, He Y, Zeng L. Particle swarm optimization algorithm with mutation operator for particle filter noise reduction in mechanical fault diagnosis. Int J Pattern Recogn Artif Intell 2020;34 (10):2058012.
[41] Cui Z, Zhang J, Wu D, Cai X, Wang H, Zhang W, Chen J. Hybrid many-objective particle swarm optimization algorithm for green coal production problem, vol. 518. Information Sciences; 2020. p. 256–71.
[42] Gurriet T, Singletary A, Reher J, Ciarletta L, Feron E, Ames A. Towards a framework for realizable safety critical control through active set invariance. In: ACM/IEEE 9th international conference on cyber-physical systems (ICCPS). IEEE; 2018, April. p. 98–106. 2018.
[43] Zhang C, Chen X. A smoothing active set method for linearly constrained non-lipschitz nonconvex optimization. SIAM J Optim 2020;30(1):1–30.
[44] Kasinathan G, Jayakumar S, Gandomi AH, Ramachandran M, Fong SJ, Patan R. Automated 3-D lung tumor detection and classification by an active contour model and CNN classifier. Expert Syst Appl 2019;134:112–9.
[45] Shi H, Wang H, Qin C, Zhao L, Liu C. An incremental learning system for atrial fibrillation detection based on transfer learning and active learning. Comput Methods Progr Biomed 2020;187:105219.
[46] Wang Y, Olaru S, Valmorbida G, Puig V, Cembrano G. Set-invariance characterizations of discrete-time descriptor systems with application to active mode detection. Automatica 2019;107:255–63.
[47] Piller O, Elhay S, Deuerlein J, Simpson A. A content-based active-set method for pressure-dependent models of water distribution systems with flow controls. J Water Resour Plann Manag 2020;146(4). 04020009-04020013.
[48] Klaučo M, Kalúz M, Kvasnica M. Machine learning-based warm starting of active set methods in embedded model predictive control. Eng Appl Artif Intell 2019;77: 1–8.
[49] Durur H, Yokuş A. Exact solutions of (2+ 1)-Ablowitz-Kaup-Newell-Segur equation. Applied Mathematics and Nonlinear Sciences 2021;6(2):381–6.
[50] Sulaiman TA, Bulut H, Baskonus HM. On the exact solutions to some system of complex nonlinear models. Applied Mathematics and Nonlinear Sciences 2021;6 (1):29–42.
[51] Sajjan K, Shah NA, Ahammad NA, Raju CSK, Kumar MD, Weera W. Nonlinear Boussinesq and Rosseland approximations on 3D flow in an interruption of Ternary nanoparticles with various shapes of densities and conductivity properties. AIMS Mathematics 2022;7(10):18416–49.
[52] Priyadharshini P, Archana MV, Ahmmad NA, Raju CSK, Yook S-J, Shah NA. Gradient descent machine learning regression for MHD flow: metallurgy process. Int Commun Heat Mass Tran 2022;138:106307.
[53] Erdogan F, Sakar MG, Saldır O. A finite difference method on layer-adapted mesh for singularly perturbed delay differential equations. Applied Mathematics and Nonlinear Sciences 2020;5(1):425–36.
[54] Sabir Z, Sakar MG, Yeskindirova M, Saldir O. Numerical investigations to design a novel model based on the fifth order system of Emden–Fowler equations. Theoretical and Applied Mechanics Letters 2020;10(5):333–42.